Okhotsk Sea and Polar Oceans Research 6 (2022) 7-18

https://doi.org/10.57287/ospor.6.7

Article

Atmospheric warming over the Barents Sea during moisture intrusion events in January 2006. Part I: Heating mechanism

Atsuyoshi MANDA[1]

[1] *Graduate School of Bioresources, Mie University*, *Tsu*, *Japan.*

(Received October 16, 2021; Revised manuscript accepted December 4, 2021)

Abstract

The mechanism of the rapid rise in air temperature in the Arctic during the recent decades remains disputed. Mechanisms proposed to explain this temperature rise include increased heat release due to sea ice loss and increased downward longwave radiation (DLR) during moisture intrusion events. This study examined the atmospheric heat and radiation budgets during moisture intrusion events in January 2006 over the Barents Sea region, through numerical simulations using the polar-optimized Weather Research and Forecasting model. No clear phase relationship was found between DLR and turbulent heat fluxes at the surface. During most events, DLR lagged the turbulent heat fluxes, indicating that DLR was not a primary driver of near-surface warming. Additionally, DLR diverged above the surface, indicating that it cooled the air column. The dominant processes of atmospheric warming during the events were vertical diffusion and heat advection, with a secondary contribution from condensational heating. The thermodynamic energy balance during the events was sensitive to static stability in the lower troposphere, suggesting the importance of sea ice loss in warming over the Barents Sea region.

Key words: Arctic amplification; surface heat flux; longwave radiation; polar WRF

1. Introduction

Over recent decades, the Arctic has been warming more rapidly than other parts of the Earth. This warming, known as Arctic amplification (AA), is more pronounced in the lower troposphere during the cold season than during other seasons. In particular, the Barents Sea region has exhibited a prominent warming trend during the past several decades (Fig. 1).

Many mechanisms have been proposed to explain AA, including increased upward longwave radiation (ULR) and turbulent heat fluxes due to sea ice decline, increased downward longwave radiation (DLR) heating due to increased water vapor and clouds, reduced outgoing longwave radiation due to a stable polar temperature profile, increased poleward energy transfer, and other processes. However, their relative importance remains unclear and under debate (Screen and others, 2018).

The contention of the leading theory on AA is that when the sea ice area declines during summer, additional heat is transferred into the ocean and this extra heat hinders the subsequent cold-season growth of sea ice, resulting in warming of the overlying atmosphere through intensified ULR and turbulent heat fluxes from open waters (*e.g.*, Screen and Simmonds, 2010). Sea ice cover in the Arctic in recent decades has exhibited a continued and drastic trend of decline. Such decline in sea ice cover affects ocean–atmosphere energy exchange, which is considered a key factor associated with AA. Recent data analysis and numerical modeling studies indicated the importance of surface fluxes in AA (*e.g.*, Isaksen and others, 2016; Dai and others, 2019). Conversely, other recent studies argued that lower-tropospheric warming in the Arctic is caused by DLR, and that surface turbulent heat fluxes are of secondary importance (*e.g.*, Gong and others, 2017; Lee and others, 2017).

Woods and Caballero (2016) showed that increase in the frequency of occurrence of intense moisture intrusion events could explain approximately half of the long-term trend in 2-m temperature over the Barents Sea. They suggested that DLR plays a fundamental role in heating the lower troposphere over the Barents Sea. In the above studies, Arctic sea ice decline is considered a consequence of atmospheric warming by DLR, not necessarily a cause (Park and others, 2015). This is in contrast to the leading theory mentioned above. Thus, the role of sea ice decline in AA remains disputed. However, these studies that highlighted the role of DLR only briefly analyzed the heating mechanism, addressing only the turbulent heat fluxes and radiative fluxes in the skin layer over the ice, snow or sea surface (the thickness of the layer was assumed to be of the order of millimeters). The heating mechanism above the surface skin layer remains unclear. To gain deeper understanding of the

mechanism of atmospheric warming that causes AA, heat budget analysis should be extended to the atmospheric column above this layer.

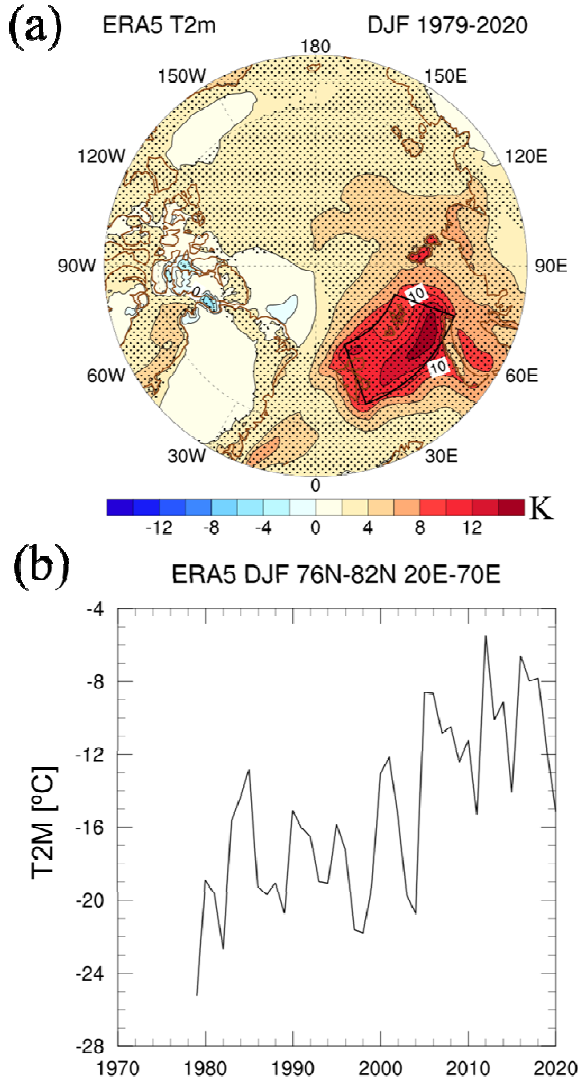

Fig. 1 (a) Map of linear trend of December-January -February (DJF) period 2-m temperature (1979–2020) in degrees kelvin [K], derived from European Centre for Medium-Range Weather Forecasts Reanalysis 5th Generation (ERA5) data. Stippled area indicates trend significant at the 5% level. (b) Time series of 2-m temperature averaged from December–February over the Barents Sea region, i.e., 76°–82°N, 20°–70°E, as indicated by black lines in (a).

The principal objective of the present study was to provide a more detailed assessment of the atmospheric response to moisture intrusion events than that conducted in earlier studies, including consideration of the vertical structure of the atmospheric warming processes above the skin layer. For example, evaluation of the terms in the thermodynamic energy equation was conducted in this study. Improved understanding of the underlying process of AA is required (Cohen and others, 2014; Dai and others, 2019), and close analysis of the associated regional and temporal variabilities helps advance comprehension of the AA mechanism. This study focused on the Barents Sea area because the warming in this region has been of greatest magnitude (Fig. 1a).

Another objective of this study was to determine the impact of changes in Arctic sea ice cover on atmospheric warming during moisture intrusion events. Analysis of this topic is addressed in a companion paper (Manda, 2022), hereafter referred to as Part II.

2. Data and Method

2.1 Atmospheric model and datasets

Numerical simulations were performed to elucidate the mechanism of atmospheric warming during moisture intrusion events. The model setup was largely similar to that used by Manda and others (2020) but with some minor modifications. Details regarding the model setup, including descriptions regarding the model domain, can be obtained from that paper.

The polar-optimized Weather Research and Forecasting model (Polar WRF; version 3.7.1), developed by Hines and Bromwich (2008), was used to perform the simulations. The horizontal grid spacing was set to 10 km and the model had 50 vertical levels up to 10 hPa. The following five schemes were used to parameterize subgrid-scale phenomena: the Morrison two-moment scheme (Morrison and others, 2009) for cloud microphysics, Mellor–Yamada–Nakanishi–Niino scheme (Nakanishii and Niino, 2009) for turbulence closure, new Kain–Fritsch scheme (Kain, 2004) for cumulus convection, and Dudhia shortwave scheme (Dudhia 1989) and a rapid radiative transfer model (Mlawer and others, 1997) for radiation.

European Centre for Medium-Range Weather Forecasts Reanalysis 5th Generation (ERA5) data (Hersbach and others, 2020) were employed for the initial and boundary conditions of the prognostic variables of the model, which included sea surface temperature (SST) and sea ice concentration. Additionally, the Modern-Era Retrospective analysis for Research and Applications, Version 2 (MERRA-2; Gelaro and others, 2017) dataset was used for evaluation of model performance. No observations were assimilated into the model and neither spectral nor grid nudging were performed.

2.2 Numerical experiments

This study focused on January 2006 for the following two reasons: this period recorded one of the warmest winters during the recent four decades (Fig. 1b), and the 2-m temperature and SST at the beginning of the cold season in 2006 were comparable to climatological values (Fig. 2). The latter is beneficial

for interpretation of the results because the influence on the simulated results of the preceding summer, which might complicate the atmospheric variations during the following winter, is expected to be minimized.

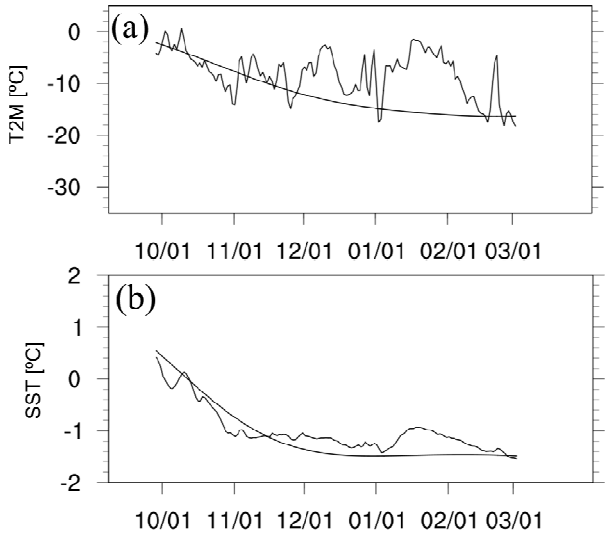

Fig. 2 Time series of (a) 2-m temperature (T2M) and (b) sea surface temperature (SST) from October 1, 2005 to February 28, 2006 averaged over the Barents Sea region (see Fig. 1 for the definition of the region). Smoothed lines indicate daily climatology data (1979–2020).

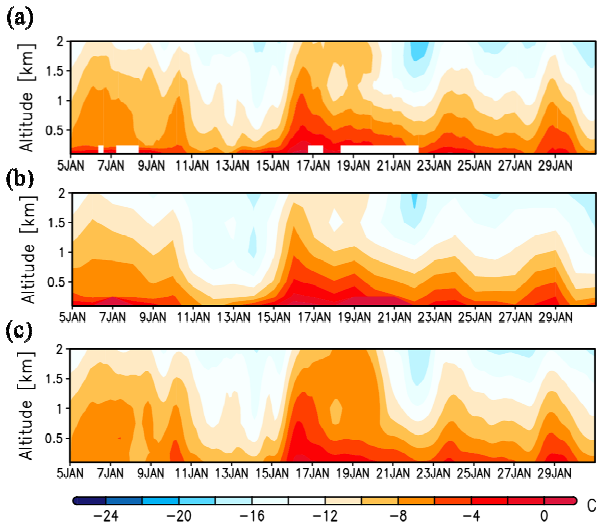

Fig. 3 Time–height diagrams of air temperature from (a) ERA5, (b) MERRA-2, and (c) the simulation conducted in this study, averaged over the Barents Sea region.

To evaluate the uncertainty resulting from internal model variability, a five-member ensemble experiment with different initiation times was conducted (Bassett and others, 2020). From 01 UTC on January 1, 2006, the time integration of each ensemble member was started at 6-h intervals until 00 UTC on January 2, 2006. From this point, all five members were run for a further 30-d period, ending at 00 UTC on January 31, 2006. The data corresponding to the period before 00 UTC on January 5, 2006 were discarded as the spin-up period, following the strategy of Bassett and others (2020). The simulated data were output for 3-h periods and the ensemble means of the output variables were used for the following analyses.

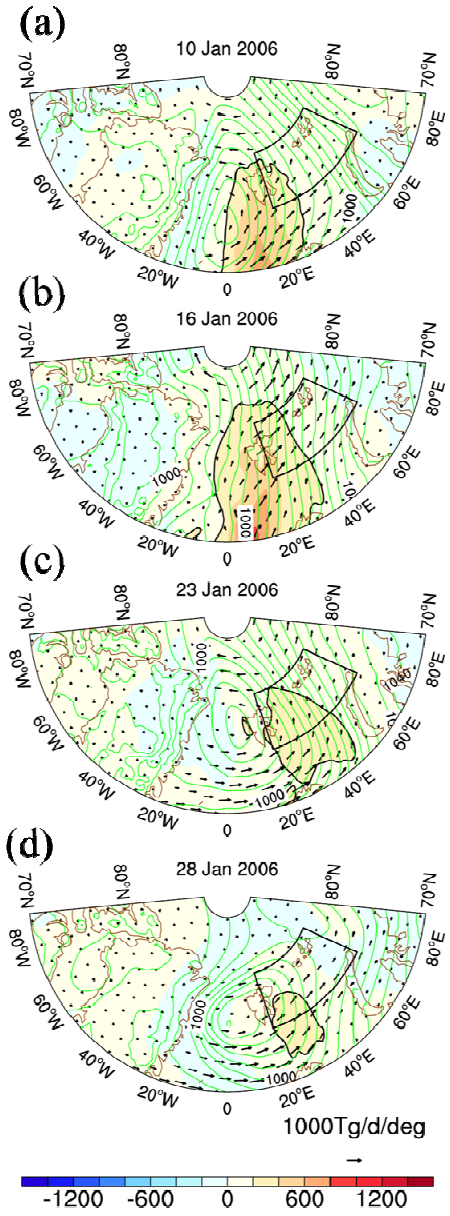

Fig. 4 Horizontal distributions of daily averaged vertically integrated moisture flux (vectors) and its northward component (colors), and sea level pressure (green contours) on January (a) 10, (b) 16, (c) 23, and (d) 28, 2006, derived from ERA5. Black contours indicate northward component of vertically integrated moisture flux of 200 in teragarm/day/degree [Tg/d/deg].

3. Results

3.1 Overview of the events

Time–height variations of air temperature averaged over the Barents Sea region (76º–82ºN, 20º–70ºE; the area enclosed by black lines in Fig. 1a) are shown in Fig. 3. Four major warming episodes can be observed in the ERA5 and MERRA-2 data: period (I) January 9–10, (II) January 15–16, (III) January 22–23, and (IV) January 28–29, 2006 (Fig. 3a and b). The model generally reproduced the variations well, including these warming episodes (Fig. 3c). Although this comparison is not a strict validation of the model using independent observational data, it represents one of the best options for assessing model performance in the Barents Sea region where the observational coverage is very sparse and limited (Rinke and others, 2006; Kohnemann and others, 2017).

These four warming episodes correspond to moisture intrusion events (Fig. 4). The black contours in Fig. 4 indicate the threshold for determining moisture intrusion events used in previous studies (Woods and others, 2013; Woods and Caballero, 2016). Overall, the northward transport of moisture during these events was attributable to southerlies that accompanied cyclones migrating along the Greenland coast from the North Atlantic toward the central Arctic, consistent with the findings of recent data analysis studies (Fearon and others, 2020; Yamanouchi, 2019, Madonna and others, 2020). As anticipated, the temporal variation of the water vapor mixing ratio over the Barents Sea corresponds well to these events (Fig. 5).

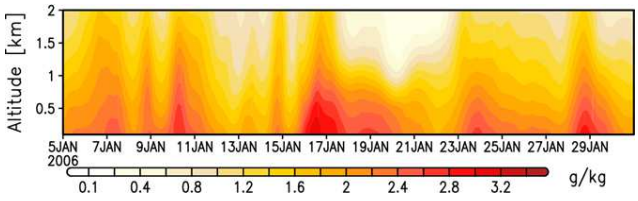

Fig. 5 Time–height cross section of water vapor mixing ratio averaged over the Barents Sea region.

3.2 Temporal variation of heating process

It is important to identify the processes governing the air temperature rises during these events. Time series of the surface fluxes averaged over the Barents Sea region are illustrated in Fig. 6. All the fluxes are defined as positive upward except for DLR, which is defined as positive downward. Although sensible heat flux (SHF) and latent heat flux (LHF) show similar variation, they do not appear linked with DLR and ULR.

It can be seen from Fig. 6 that SHF started to rise around January 7 and reached its first peak around January 14. It subsequently dropped sharply to reach a minimum value around January 16. Then, SHF increased again to reached its second peak around January 22, fell gradually until January 29, and then increased to reach its third peak around January 30. The variation of LHF was similar to that of SHF.

It can also be seen from Fig. 6 that DLR started to decrease around January 10 and continued to fall gradually with small fluctuation until reaching its local minimum around January 16. It then increased sharply after January 16 to reach its peak around January 17. It subsequently declined slowly with small fluctuation until January 22, following which it showed slight increase to reach a plateau that was maintained until January 27. It then started climbing again and reached another peak around January 29. Conversely, ULR remained almost constant throughout the analysis period.

As described in the above analysis, there is no clear phase relationship between DLR and other fluxes. The peak of both SHF and LHF preceded that of DLR during periods (II) and (III). If DLR drives surface heating, it should precede SHF and LHF, which is evidently not the case during these periods. The peak of both SHF and LHF followed that of DLR during period (IV), suggesting that the mechanism of near-surface warming during period (IV) differed from that of periods (II) and (III).

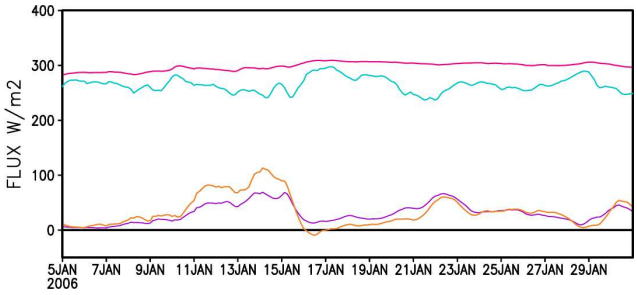

Fig. 6 Time series of DLR (cyan), ULR (magenta), SHF (orange), and LHF (purple) averaged over Barents Sea Region.

Time–height diagrams of the terms in the thermodynamic equation averaged over the Barents Sea region (indicated by the black lines in Fig. 1a) are presented in Fig. 7. Shortwave radiation is omitted from this figure because the simulation corresponded to the polar night period. The residual term was almost zero and therefore it also is not shown.

Near-surface warming (<0.5 km) is primarily due to vertical diffusion acting to transmit the upward SHF (Fig. 7b), because the SST is higher than the surface air temperature over open water in the Barents Sea region during most of January (Fig. 2). The advection term also contributed to the warming except for the near surface in period (I), and the first half of periods (II) and (III). Condensational heating by the cloud microphysics scheme led to slight cooling just above

the surface, whereas the cumulus convection scheme contributed to warming.

Warming above 0.5 km height is attributable to advection with a slight contribution to heating by the cloud microphysics and cumulus convection schemes. Interestingly, net longwave radiation (the sum of ULR and DLR) cools the atmosphere. Because this result appears inconsistent with recent studies (*e.g.*, Gong and others, 2017), the reason for this is examined by assessing DLR and ULR separately.

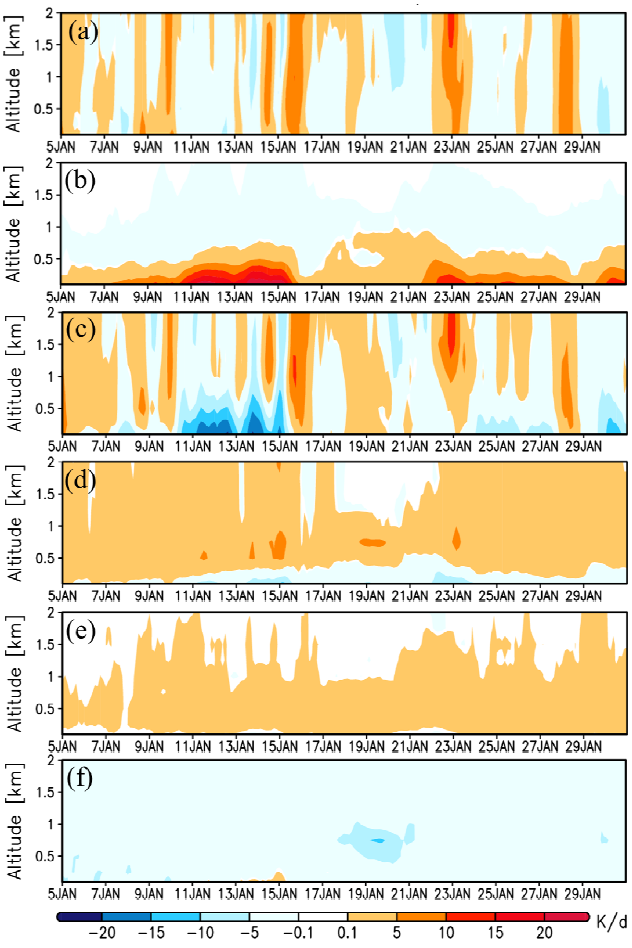

Fig. 7 Time–height cross sections of (a) tendency, (b) vertical diffusion, (c) advection, (d) cloud microphysics, (e) cumulus convection, and (f) radiation terms in the thermodynamic energy equation averaged over the Barents Sea region.

The radiative budget above 0.1 km height averaged over the Barents Sea region is shown in Fig. 8. The vertical distribution of DLR exhibits a bottom-intensified pattern that reaches its peak in the lowest layer throughout the analysis period (Fig. 8a), leading to divergence of DLR and cooling of the atmospheric column (Fig. 8b). Recent studies suggest that longwave radiation is one of the major contributors to atmospheric warming over the Barents Sea region during winter (Woods and others, 2013; Woods and Caballero, 2016; Gong and others, 2017), which contrasts with the findings of this study. However, the previous studies examined DLR only in the surface skin layer. The value of DLR in that layer is not directly related to heating of the air column, whereas its convergence is relevant to such heating. In contrast to DLR, ULR can be seen to converge and thereby it contributed to warming (Fig. 8c). However, its magnitude was smaller than that of ULR; hence, the negative net longwave radiation (i.e., cooling), as shown in Fig. 7f.

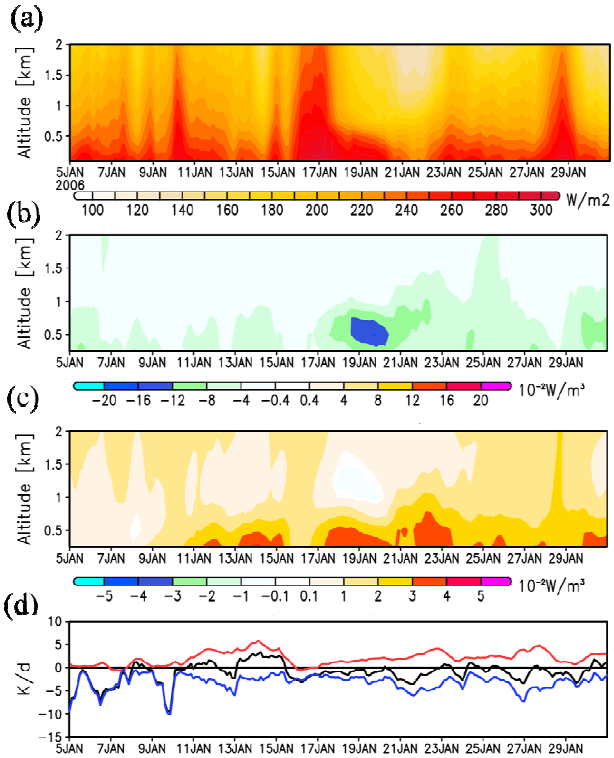

Fig. 8 Time–height cross sections of (a) DLR and vertical convergences of (b) DLR and (c) ULR. (d) Time series of vertical convergences of ULR (red), DLR (blue), and ULR (black) minus DLR in the lowest 0.1 km above the surface.

In summary, the heat budget analysis indicates that the dominant terms for atmospheric heating during the intrusion events are vertical diffusion and advection, with a slight contribution from condensational heating. Additionally, although ULR contributes to warming, its effect is canceled out by DLR. Previous studies showed that the warmth found in the Arctic Ocean is maintained primarily by horizontal cold advection countered by diabatic heating (Deser and others, 2010; Serreze and others, 2011), which is not necessarily the case in this study. The findings of this study indicate that advection does not always counteract vertical diffusion, but does contribute to near-surface warming

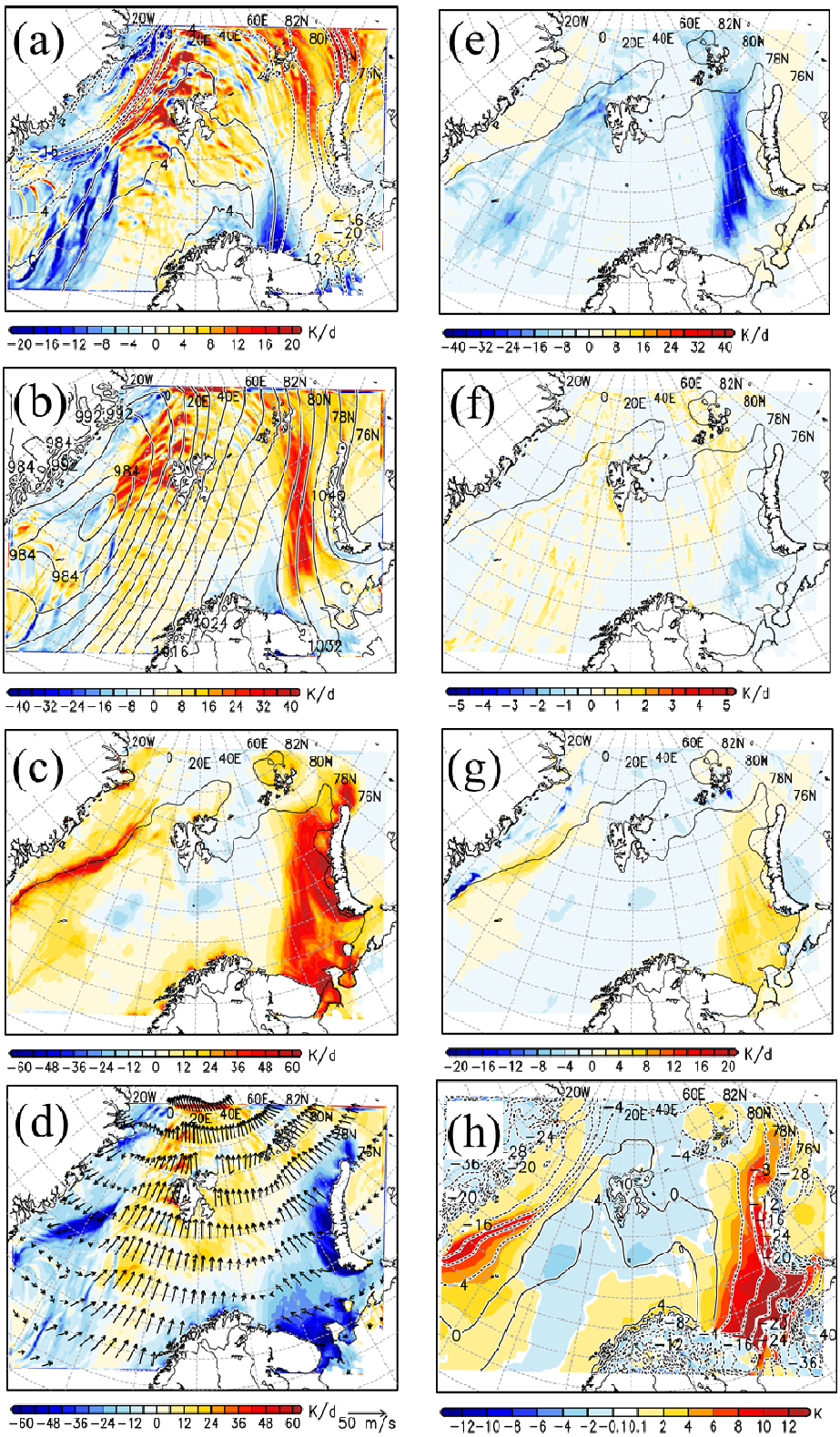

Fig. 9 Horizontal distributions of (a) tendency, (b) sum of advection and vertical diffusion, (c) vertical diffusion, (d) advection, (e) cloud microphysics, (f) cumulus convection, and (g) radiation terms in the thermodynamic energy equation, and (h) difference between skin and 2-m temperatures at 0.1 km height (colors), averaged from 12 UTC on January 15 to 00 UTC on January 16, 2006. Contours in (a), (b), and (c), (e), (f), and (g) indicate 2-m temperature (ºC), sea level pressure (hPa), and sea ice concentration of 0.2, respectively. Vectors in (d) indicate wind velocity.

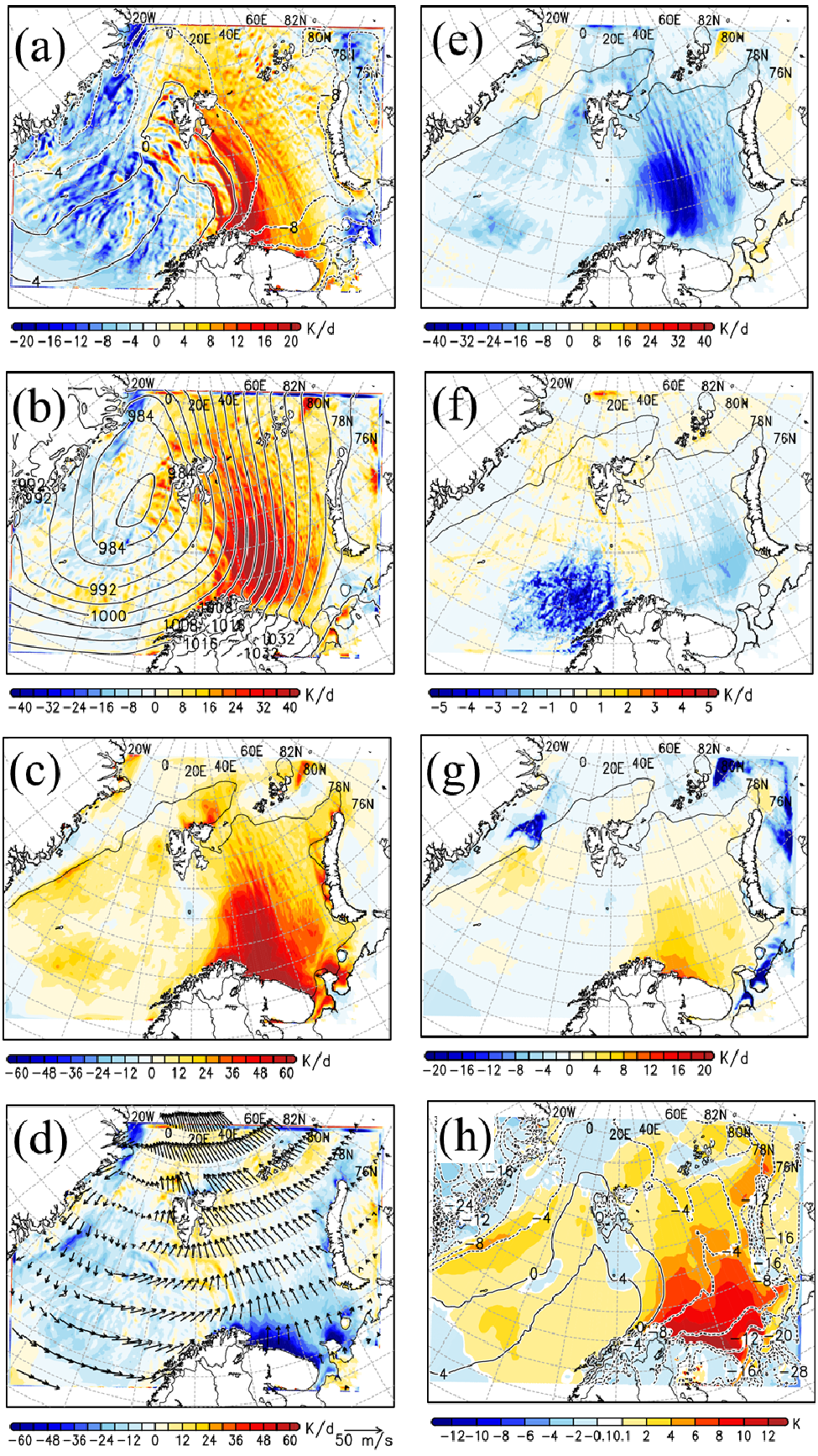

Fig. 10 Same as Fig. 9 but averaged from 18 UTC on January 22 to 06 UTC on January 23, 2006.

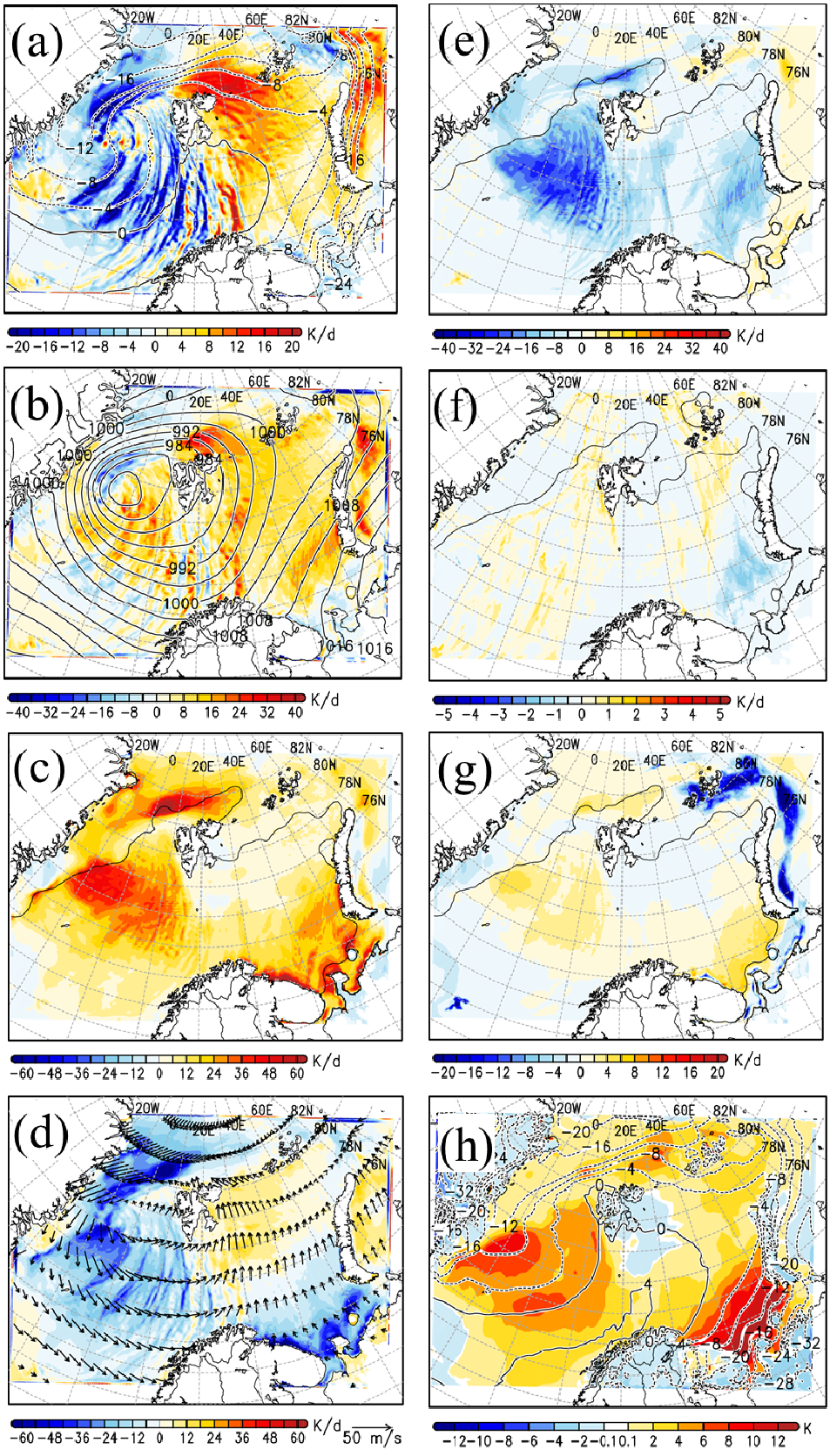

Fig. 11 Same as Fig. 9 but averaged from 00 UTC on January 28 to 12 UTC on January 28, 2006.

in some cases. The relative roles of the various processes in the thermodynamic energy balance atmospheric warming are thus explored further in the next section.

3.3 Spatial variation of heating process

The horizontal distributions of the terms in the thermodynamic energy equation at the height of 0.1 km during period (II) are shown in Fig. 9a. The data were averaged over the 12-h period from 12 UTC on January 15 to 00 UTC on January 16, 2006.

The tendency (rate of temporal change) term exhibited overall heating over the Barents Sea region except for some areas including the area around the northwestern corner of the region (Fig. 9a). This geographical pattern is reasonably explained by the sum of the advection and vertical diffusion terms (Fig. 9b). In addition to the area north of Franz Josef Land, the vertical diffusion term dominated in the region west of Novaya Zemlya (Fig. 9c). A cold air mass whose temperature was much lower than that of the skin temperature in the region induced heating due to vertical diffusion (Fig. 9c). Conversely, domination by the advection term and a warm air mass from the North Atlantic appear to be the primary influences on air temperature in the western portion. A low–high-pressure system located over the east coast of Greenland and east of Novaya Zemlya caused a strong zonal pressure gradient and associated winds that led to warm advection (Gong and Luo, 2017; Yamanouchi, 2019). Spatial variations similar to those described here were observed during period (I) (the figure not shown).

Horizontal distributions of diabatic terms such as the cloud microphysics, cumulus convection, and radiation terms in the surface boundary layer were strongly influenced by surface conditions (Fig. 9e–h). The spatial variation of the radiation term (Fig. 9g) was reasonably similar to that of the difference between the surface skin and 2-m temperatures. This is reasonable because ULR (DLR) contributed to warming (cooling) over most of the domain (the figure not shown). The horizontal distribution of cloud microphysics (Fig. 9e) was also reasonably similar to that of the negative of the difference between the surface skin and 2-m temperatures (Fig. 9h). Although the magnitude is much smaller than that of the cloud microphysics, the horizontal distribution of the cumulus convection term also exhibited a similar distribution.

During period (III), vertical diffusion was the main contributor to warming over the Barents Sea region (Fig. 10). The advection term cooled the atmosphere over most of the Barents Sea region. In contrast to period (II), southeasterlies dominated and brought cold air from the northern coasts of both Norway and Russia. The sea level pressure distribution during this period was rather different to that of period (II). The cyclone located over the Greenland Sea during this period was much larger than that during period (II), and its center was located slightly further east than that of the low observed in period (II). These differences caused the isobars to be aligned more in the north–south direction over the Barents Sea, in comparison with the isobars in period (II), which induced movement of cold air from the northern coast of the Scandinavian Peninsula to the Barents Sea (Fig. 10d). Similar to period (II), the near-surface static stability strongly affected the horizontal distributions of the cloud microphysics, cumulus convection, and radiation terms during this period.

In contrast to period (III), the advection term dominated during period (IV) (Fig. 11). A high pressure system located east of Novaya Zemlya during this period was weaker in comparison with the high in the other periods. Warm advection due to the cyclone located over the Greenland Sea affected atmospheric warming over the Barents Sea region more directly than in the other periods (Fig. 11a). The intensified vertical diffusion southwest of Svalbard in the Greenland Sea could have contributed to the formation of a warm air mass (Fig. 11c) and hence remotely influenced warm advection over the Barents Sea region (Fig. 11d).

The horizontal distribution of each of the cloud microphysics and cumulus convection terms was similar to that of the negative of the difference between the surface skin and 2-m temperatures. The horizontal distribution of the radiation term was similar to that of difference between the surface skin and 2-m temperatures, as in the other periods, except for areas to the east and north of Novaya Zemlya (Fig. 11g). Cooling by DLR dominated the warming by ULR in these areas (figure not shown).

As expected, the horizontal variation of the vertical diffusion term is strongly controlled by the static stability near the surface, as indicated by the difference between the skin and 2-m temperatures. It is also suggested that the advection term is affected by the temperature of the air intruded from lower latitudes. The relative importance of vertical diffusion and advection on atmospheric warming is sensitive to these factors. Recent studies highlighted the remote influence of the humidity and temperature of air masses from lower latitudes on atmospheric warming in the Arctic (*e.g.*, Gong and others, 2017). Conversely, this study highlighted the importance of local atmospheric and oceanic conditions during moisture intrusion events. The spatiotemporal variabilities of temperatures around the Barents Sea region are important controlling factors of the heating mechanism during the events.

4. Summary and Discussion

Recent studies suggested that the DLR that accompanies a moisture intrusion event is a main

contributor to atmospheric warming over the Barents Sea region during winter. This study examined the heating mechanism during such events using numerical simulations. Heat budget analysis indicated that the vertical diffusion term is one of the main contributors to atmospheric warming in the lower troposphere during intrusion events. Conversely, the advection term was found to contribute to atmospheric warming in some cases and to cooling of the atmosphere in other cases. Cloud microphysics and cumulus heating also contribute to the warming, but they are of secondary importance. No single dominant mechanism could be attributed to the atmospheric warming during the periods examined in this study.

The relative importance of the advection and vertical diffusion terms depends on the specific event. This is important for understanding the mechanism of AA. Dominance of the former implies the importance of remote influences from lower latitudes, whereas dominance of the latter suggests the importance of more local influences around the Barents Sea region.

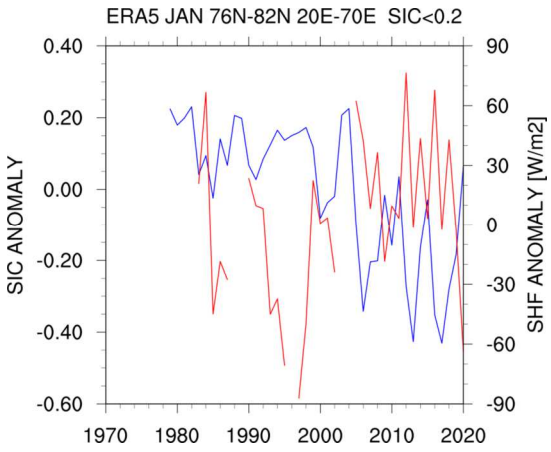

Fig. 12 Time series of monthly anomalies of sea ice concentration (SIC; blue) averaged over the Barents Sea region and sensible heat flux (SHF; red) averaged over the area where SIC is <0.2 in the Barents Sea region.

It might be considered unexpected that longwave radiation did not dominate the atmospheric warming during the period examined in this study. The sea ice concentration in January 2006 recorded one of the smallest values since 1979, and SHF over the open water was reasonably large (Fig. 12). Therefore, a large amount of heat could have been supplied from the open water to the overlying atmosphere around the Barents Sea region during the intrusion events, which would have contributed to strong vertical diffusion of heat. The heating due to vertical diffusion could have been much larger than in a normal year under such environmental conditions. Although this work is a case study that focused on a few specific events, it should be extended to other events in various environments to obtain comprehensive understanding of atmospheric warming over the Barents Sea region during winter. In particular, the impact of sea ice cover on the heat budgets is explored in Part II.

The heat budget analysis also showed that net longwave radiation cooled the air column. It was attributed to the vertical profile of DLR, which was bottom-intensified and diverged vertically. Although ULR converged and heated the air column in the lower troposphere, its magnitude was smaller than that of DLR. Thus, the combination of DLR and ULR contributed to cooling. This result appears inconsistent with the findings of previous studies. For example, on the basis of analysis of the data obtained during winter 1996/1997 through the Surface Heat Budget of the Arctic Ocean Program (Uttal and others, 2002), Stramler and others (2011) argued that DLR played a primary role in heating the atmosphere. It should be noted that they analyzed DLR only over the surface. One possible reason for the difference could be differences in the vertical profiles of air temperature. A strong surface-based inversion was observed during most of the analysis period of Stramler and others (2011). In contrast, such an inversion was absent over the Barents Sea region in January 2006 (Fig. 3). Longwave radiation can be influenced by many factors such as the liquid and ice water paths, cloud base height, and cloud optical depth (*e.g.*, Barton and Veron, 2012), all of which are strongly influenced by the vertical profile of air temperature. The relationships among the vertical profiles of temperature, hydrometeors, and DLR are discussed in Part II. It should be noted that more comprehensive studies highlighting the vertical distribution of DLR are needed to clarify the role of DLR in atmospheric warming because the convergence of DLR is directly related to the heating of the air column.

All of the events examined in this study were associated with northward migration of cyclones over the Greenland Sea from the North Atlantic toward the central Arctic, which is consistent with recent studies (*e.g.*, Madonna and others, 2020; Fearon and others, 2021). The results of this study also indicated that slight differences in the paths and dimensions of such cyclones could modify the heating mechanism over the Barents Sea region through changes in the temperature and wind fields. Although changes in cyclonic activity over the Barents Sea region remains a matter of debate (Koyama and others, 2017), a recent data analysis study indicated that reduced sea ice cover is related not only to more frequent occurrence of cyclones but also to stronger cyclones (Valkonen and others, 2021). A recent modeling study suggested that increase in oceanic heat transport across the Barents Sea openings from the North Atlantic increases the frequency of occurrence of intense cyclones (Akperov and others, 2020). These

changes in cyclone characteristics could affect atmospheric warming over the Barents Sea and should be explored in future studies.

As mentioned above, the thermodynamic energy balance during the intrusion events is sensitive to near-surface stability. One of the most important factors to affect near-surface stability around the Barents Sea region is the horizontal distribution of sea ice cover, which is examined in the companion paper (Part II).

Acknowledgments

The author thanks Dr. D. H. Bromwich and the Polar Meteorology Group, Byrd Polar and Climate Research Center, Ohio State University for providing the Polar WRF. This work was supported in part by the Arctic Challenge for Sustainability II (ArCS II) Project (Program Grant Number JPMXD1420318865), the Japan Society for Promotion of Science through Grants-in-Aid for Scientific Research (Grant Numbers JP17H02958 and JP19H05697), and the Collaborative Research Program of the Research Institute for Applied Mechanics, Kyushu University (Grant Number 2021 S3-3). We thank James Buxton MSc of Edanz (https://jp.edanz.com/ac) for editing a draft of this manuscript.

References

Akperov, M., V.A. Semenov and 4 others (2020): Impact of Atlantic water inflow on winter cyclone activity in the Barents Sea: Insights from coupled regional climate model simulations. *Env. Res. Lett*., **15**: 024009, doi:10.1088/1748-9326/ab6399.

Barton, N.P, Veron D.E. (2012): Response of clouds and surface energy fluxes to changes in sea-ice cover over the Laptev Sea (Arctic Ocean). *Clim. Res*., **54**: 69-84.

Bassett, R., P.J. Young and 3 others (2020): A large ensemble approach to quantifying internal model variability within the WRF numerical model. *J. Geophys. Res. Atmos.*, **125**: e2019JD031286.

Cohen, J. and J. Screen and 9 others (2014): Recent Arctic amplification and extreme mid-latitude weather, *Nat. Geosci*., **7**: 627–637.

Dai, A., D. Luo and 2 others (2019): Arctic amplification is caused by sea-ice loss under increasing CO_2. *Nat. Commun.*, **10**: 121, doi:10.1038/s41467-018-07954-9.

Deser, C., R. Tomas and 2 others (2010): The seasonal atmospheric response to projected Arctic sea ice loss in the late twenty-first century. *J. Clim*., **23**: 333–351.

Dudhia, J. (1989): Numerical study of convection observed during the Winter Monsoon Experiment using a mesoscale two-dimensional model. *J. Atmos. Sci*., **46**: 3077–3107.

Fearon, G.F, J.D. Doyle and 3 others (2021): The role of cyclones in moisture transport into the Arctic. *Geophys. Res. Lett*., **48**: e2020GL090353.

Gelaro, R., W. McCarty and 29 others (2017): The modern-era retrospective analysis for research and applications, version 2 (MERRA-2). *J. Clim*., **30**: 5419-5454.

Gong, T., S. Feldstein, and S. Lee (2017): The role of downward infrared radiation in the recent Arctic winter warming trend, *J. Climate*, **30**: 4937-4949.

Gong, T. and Luo (2017): Ural blocking as an amplifier of the Arctic sea ice decline in winter, *J. Climate*, **30**:, 2639-2654.

Hersbach, H., B. Bell and 42 others (2020): The ERA5 global reanalysis. *Q.J.R. Meteorol. Soc*., **146**: 1999–2049.

Hines, K.M. and D.H. Bromwich (2008): Development and testing of polar weather research and forecasting (WRF) model. Part I: Greenland ice sheet meteorology. *Mon. Weather Rev*., **136**: 1971–1989.

Isaksen, K., Ø. Nordli and 4 others (2016): Recent warming on Spitsbergen—Influence of atmospheric circulation and sea ice cover, *J. Geophys. Res*, **121**: 11,913– 11,931.

Kain, J.S. (2004): The Kain-Fritsch convective parameterization: an update. *J. Appl. Meteor*., **43**: 170–181.

Kohnemann, S.H.E., G. Heinemann and 2 others (2017): Extreme warming in the Kara Sea and Barents Sea during the winter period 2000–16, *J. Climate*, **30**: 8913-8927.

Koyama, T., J. Stroeve and 2 others (2017): Sea ice loss and Arctic Cyclone Activity from 1979 to 2014. *J. Climate*, **30**: 4735–4754.

Lee, S., T. Gong, T. and 3 others (2017): Revisiting the cause of the 1989–2009 Arctic surface warming using the surface energy budget: Downward infrared radiation dominates the surface fluxes. *Geophys. Res. Lett*., **44**: 10,654– 10,661.

Madonna, E., H. Gabriel and 3 others (2020): Control of Barents Sea wintertime cyclone variability by large-scale atmospheric flow. *Geophys. Res. Lett*., **47**: e2020GL090322.

Manda, A., T. Mitsui and 4 others (2020): Storm-mediated ocean–atmosphere heat exchange over the Arctic Ocean: A case study of a Barents Sea cyclone observed in January 2011. *OSPOR*, **4**: 1–9.

Manda, A. (2022): Atmospheric warming over the Barents Sea during intense moisture intrusion events in January 2006. Part II: Impact of sea ice decline. *OSPOR*, **6**: 19-26.

Mlawer, E.J., S.J. Taubman and 3 others (1997): Radiative transfer for inhomogeneous atmospheres: RRTM, a validated correlated-k model for the longwave. *J. Geophys. Res*., **102**: 16663-16682.

Morrison, H., G. Thompson and V. Tatarskii (2009): Impact of cloud microphysics on the development of trailing stratiform precipitation in a simulated squall line: comparison of one- and two-moment schemes. *Mon. Wea. Rev*., **137**: 991-1007.

Nakanishi, M. and H. Niino (2009): Development of an improved turbulence closure model for the atmospheric boundary layer. *J. Meteorol. Soc. Jpn*., **87**: 895-912.

Park, D.-S., S. Lee and S.B Feldstein (2015): Attribution of the recent winter sea ice decline over the Atlantic sector of the Arctic Ocean, *J. Climate*, **28**: 4027-4033.

Rinke, A., W. Maslowski and 2 others (2006): Influence of sea ice on the atmosphere: A study with an Arctic atmospheric regional climate model, *J. Geophys. Res*., **111**: D16103, doi:10.1029/2005JD006957.

Screen, J.A., C. Deser and 10 others (2018): Consistency and discrepancy in the atmospheric response to Arctic sea-ice loss across climate models. *Nat. Geosci*., **11**: 155–163.

Screen, J.A. and I. Simmonds (2010): The central role of diminishing sea ice in recent Arctic temperature amplification. *Nature*, **464**: 1334–1337.

Serreze, M.C., A.P. Barrett and J.J. Cassano (2011): Circulation and surface controls on the lower tropospheric air temperature field of the Arctic. *J. Geophys. Res*., **116**: D07104, doi: 10.1029/2010JD015127.

Stramler, K., A.D. Del Genio, and W.B. Rossow (2011): Synoptically driven Arctic winter states. *J. Climate*, **24**: 1747-1762.

Uttal, T., J.A. Curry and 21 others (2002): Surface heat budget of the Arctic Ocean. *Bull. Am. Meteorol. Soc*., **83**: 255-275.

Valkonen, E., J. Cassano and E. Cassano (2021): Arctic cyclones

and their interactions with the declining sea ice: a recent climatology. *J. Geophys. Res*., **126**, e2020JD034366.

Woods, C., R. Caballero, and G. Svensson (2013): Large-scale circulation associated with moisture intrusions into the Arctic during winter. *Geophys. Res. Lett*., **40**: 4717–4721.

Woods, C. and R. Caballero (2016): The role of moist intrusions in winter Arctic warming and sea ice decline, *J. Climate*, **29**: 4473-4485.

Yamanouchi, T. (2019): Arctic warming by cloud radiation enhanced by moist air intrusion observed at Ny-Ålesund, Svalbard, *Polar Sci*., **21**: 110-116.

Correspondence to: A. Manda, am@bio.mie-u.ac.jp